Pet.Sci.(2012)9:379-388
DOI 10.1007/s12182-012-0222-9


# Structure optimization of gas-liquid combined loop reactor using a CFD-PBE coupled model

**Qi Nana[1], Zhang Kai[1]*, Xu Gang[1], Yang Yongping[1] and Zhang Hu[2]**

[1] School of Energy Power and Mechanical Engineering, North China Electric Power University, Beijing 102206, China
[2] School of Chemical Engineering, University of Adelaide, South Australia, SA 5005, Australia



**Abstract:** Flow characteristics, such as flow pattern, gas holdup, and bubble size distribution, in an internal loop reactor with external liquid circulation, are simulated to investigate the influence of reactor internals by using the computational fluid dynamics (CFD)-population balance equations (PBE) coupled model. Numerical results reveal that introducing a downcomer tube and a draft tube can help to improve the mass and heat transfer of the reactor through enhanced liquid circulation, increased gas holdup and reduced bubble diameter. The hydrodynamic behavior in the internal loop reactor with external liquid circulation can be managed effectively by adjusting the diameter and axial position of the draft tube.

**Key words:** Loop reactor, Structure optimization, Hydrodynamics, CFD-PBE coupled model

## 1 Introduction

Loop reactors have been widely used in chemical processing and other related processes due to their simple construction without moving parts, excellent mass and heat transfer, efficient mixing with low energy consumption, straightforward low cost operation and so on (Deng et al, 2010). Generally, the loop reactors can be divided into internal and external loop reactors. The internal loop reactor is usually constructed by mounting a draft tube inside a bubble column. Liquid is brought up by gas sparged into the draft tube (riser) or the annulus (downcomer) region and falls down due to gravity, which results in overall liquid circulation in the column. On the other hand, the external loop reactor has an external downcomer attached to a bubble column. Gas is dispersed at the bottom of the riser and a global liquid circulation is induced due to the pressure difference between the riser and the downcomer. The design and optimization of these reactors is a key issue for applying them in new fields. In recent years, several modified configurations of loop reactors were proposed to meet the requirement for alkylation processes and liquid fuel synthesis. (Liu et al, 2007; Lu et al, 2009; Zhang et al, 2003; Zhang and Zhao, 2006). Among these reactors, the combined gas-liquid (or slurry) loop reactor proposed by Lu et al (2009) makes use of the advantages of the external or internal loop reactor, in addition, it includes a liquid (or slurry) spray section in the upper part, sieve plates in the middle part, and an internal loop section in the lower part (Lu et al, 2009; Zhang et al, 2010b). As shown in Fig.1, external liquid circulation is introduced by a downcomer tube, which enhances the driving force due to the pressure difference between the riser and the annular region and increases the interfacial area between the gas and liquid phases.

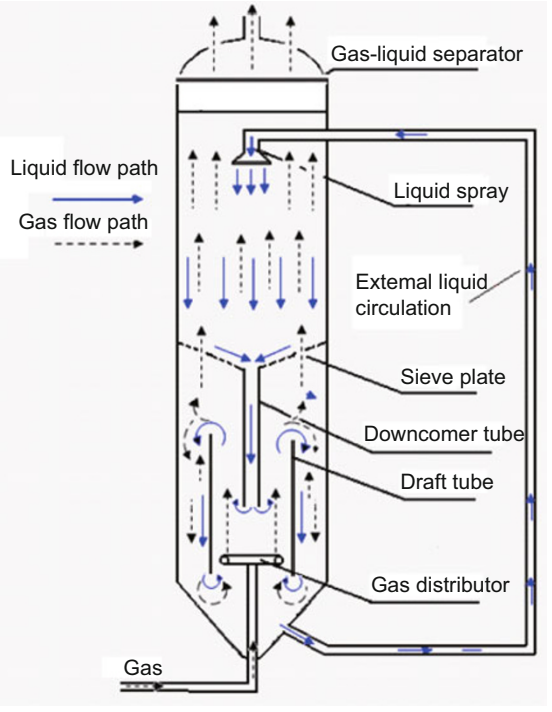


**Fig. 1** Schematic diagram of an internal loop reactor with external liquid circulation

For this proposed combined loop reactor, the internal geometry may significantly influence the hydrodynamics and chemical reactions. It has been reported for the loop reactors that internal geometry and hydrodynamics are inter-related and their relationship can be quite complex (Šimčík

*Corresponding author. email: zhangk98@yahoo.com
Received January 6, 2012

et al, 2011). For example, Nishikawa et al (1976) reported that, for efficient spouting, the ratio between the diameter of the cone bottom and the column diameter should be smaller than 0.2. Kolde et al (1983) investigated the effect of the ratio between the diameters of the draft tube and the column diameter ($D_T/D$) on the hydrodynamics of the air-water system, and the result demonstrated that in the range of $0.5 < D_T/D < 0.75$, a decrease in $D_T/D$ will result in an increase in the gas-liquid mass transfer coefficient but no significant change in the global gas hold-up. Hwang and Fan (1986) used draft tube bubble columns with $D_T/D$ ratio of 0.50, 0.67 and 0.83, and found that a $D_T/D$ ratio of 0.50 yielded the largest global gas hold-up. Wachi et al (1991) reported that, with $D_T/D$ increase, the gas hold-up between the draft tube and annular regions increased. Saez et al (1995) found that the axial position of the draft tube can efficiently control the hydrodynamic behavior of these reactors. Hekmat et al (2010) chose a distance of 0.05 m between the draft tube and the wall as the optimum distance as it modified the performance of the reactor. To optimize the design of the combined loop reactors, a better understanding of the physical mechanisms at the local scale is needed (Ayed et al, 2007). Generally, there are two ways to obtain local physical mechanisms: One is to utilize empirical correlations obtained from experimental data (Heyouni et al, 2002; Giovannettone and Gulliver, 2008; Gandhi et al, 2009); the other is to apply mathematical models based on computational fluid dynamics (CFD). Empirical correlations are applicable only in a limited range of geometric and operating parameters and extrapolation of them is very risky. Therefore, the hydrodynamics in the loop reactors have been simulated extensively (such as by Krishna et al, 1999; Chen et al, 2005; Dhotre and Joshi, 2007; Hekmat et al, 2010).

Even though the aforementioned achievements have been made, in most reports dealing with gas-liquid flows, gas bubble size is assumed to be the same, i.e. the mono-dispersed gas bubbles (Krishna et al, 1999; Chen et al, 2005; Dhotre and Joshi, 2007; Hekmat et al, 2010; Šimčík, 2011). Actually, in dispersed gas-liquid flow, a wide range of bubble sizes and shapes exist at different locations throughout the whole reactor. It is of importance to take breakage and coalescence effects into consideration and predict the local gas bubble size distribution. With a multiple size group (MUSIG) model, bubble sizes are calculated directly from the population balance equations (PBE) and bubble-bubble interactions are controlled by bubble coalescence and breakup law (Bhole et al, 2008; Jia et al, 2007; Zhang et al, 2010a). In our work, systematic and detailed investigation of the gas-liquid flow behavior (liquid velocity, local gas holdup and bubble size distributions) and the effects of reactor internals (downcomer tube and draft tube) on the hydrodynamics in the novel internal loop reactor with external liquid circulation are carried out by using the CFD-PBE coupled model.

## 2 CFD model

### 2.1 Continuity and momentum equations

An Eulerian-Eulerian multi-fluid model is employed, where gas and liquid phase are treated as continua, interpenetrating and interacting with each other in the computational domain. The pressure field is assumed to be shared by both phases, in proportion to their respective volume fraction. The motion of each phase is governed by corresponding mass and momentum conservation equations.

The continuity equation is:

$$\frac{\partial(\alpha_i\rho_i)}{\partial t}+\nabla\cdot(\alpha_i\rho_i\vec{u}_i)=0 \tag{1}$$

where $\alpha$, $\rho$ and $u$ are volume fraction, density and velocity, respectively. The subscript $i$ stands for gas or liquid phase.

The momentum equation is:

$$\begin{aligned}&\frac{\partial(\alpha_i\rho_i\vec{u}_i)}{\partial t}+\nabla\cdot(\alpha_i\rho_i\vec{u}_i\vec{u}_i)\\&=-\alpha_i\nabla P_i+\nabla\cdot(\alpha_i\mu_i(\nabla\vec{u}_i+(\nabla\vec{u}_i)^{\mathrm{T}}))+\vec{F}_i+\alpha_i\rho_i\vec{g}\end{aligned} \tag{2}$$

where $P$, $\mu$, and $g$ are pressure, dynamic viscosity and gravity acceleration, respectively. $F_i$ is the interfacial force acting on phase $i$ due to the presence of the other phase, which includes drag force, interphase turbulent dispersion force, virtual mass and lift force. Virtual mass and lift force are neglectable in comparison with the drag force and interphase turbulent dispersion force (Bartrand et al, 2009; Panneerselvam et al, 2008) and they are excluded in the interfacial force, $F_i$:

$$\vec{F}_i=\vec{F}_i^{\mathrm{D}}+\vec{F}_i^{\mathrm{T}} \tag{3}$$

where $F_i^D$ is the drag force, and $F_i^T$ is the interfacial force due to turbulent dispersion.

The drag component of the interfacial force term is given by

$$\vec{F}_i^{\mathrm{D}}=\frac{C_{\mathrm{D}}}{8}A_{ij}\rho_i\left|\vec{u}_j-\vec{u}_i\right|(\vec{u}_j-\vec{u}_i) \tag{4}$$

where $C_D$ is the drag force coefficient, $A_{ij}$ is the net interfacial area between the two phases. The Grace model proposed by Cift et al (1978) is chosen for calculating the drag force, and the drag force coefficient is:

$$C_{\mathrm{D}}=\frac{4}{3}\frac{gd_{\mathrm{b}}}{u_{\mathrm{T}}^2}\frac{\Delta\rho}{\rho_{\mathrm{l}}} \tag{5}$$

where $d_b$ stands for the mean bubble diameter, $\Delta\rho$ is the density difference between the liquid and gas phases, $u_T$ is the bubble terminal rise velocity, which can be calculated as:

$$u_{\mathrm{T}}=\frac{u_{\mathrm{l}}}{\rho_{\mathrm{l}}d_{\mathrm{b}}}M^{-0.149}(J-0.857) \tag{6}$$

$M$ as the Morton number (a fluid property) is:

$$M=\frac{u_{\mathrm{l}}^4g\Delta\rho}{\rho_{\mathrm{l}}^2\sigma^3} \tag{7}$$

where $\sigma$ is surface tension
and $J$ is given by:

$$J=0.94H^{0.751}\qquad 2<H\leq 59.3 \tag{8}$$

$$J=3.42H^{0.441}\qquad H>59.3 \tag{9}$$

In Eqs.(8) and (9), $H$ is calculated as:

$$H = \frac{4}{3} E\ddot{o}\, M^{-0.149} \left(\frac{\mu_l}{\mu_{ref}}\right)^{-0.14} \tag{10}$$

where $\mu_{ref}$ is the molecular viscosity of tap water at a reference temperature and pressure; $E\ddot{o}$ stands for Eötvös number as below:

$$E\ddot{o} = \frac{g\Delta\rho d_b^2}{\sigma} \tag{11}$$

The turbulent dispersion force, $\vec{F}_i^T$, is calcuated by the Lopez de Bertodano model (1991):

$$\vec{F}_i^{\mathrm{T}} = C_{\mathrm{TD}} C_{\mathrm{D}} \frac{\nu_{\mathrm{tl}}}{\sigma_{\mathrm{tl}}} \left(\frac{\nabla \alpha_{\mathrm{g}}}{\alpha_{\mathrm{g}}} - \frac{\nabla \alpha_{\mathrm{l}}}{\alpha_{\mathrm{l}}}\right) \tag{12}$$

where $C_{\mathrm{TD}}$, the momentum transfer coefficient for the interphase drag force, has a value of 0.1 to 0.5 based on the superficial gas velocity; $C_{\mathrm{D}}$ stands for drag force coefficient, $\nu_{\mathrm{tl}}$ and $\sigma_{\mathrm{tl}}$ for turbulent viscosity and turbulent Schmidt number of the liquid phase, respectively.

### 2.2 Turbulence model

In order to solve the Reynolds stress in the turbulent momentum equations, the standard $k$–$\varepsilon$ model is chosen for simulating the liquid phase, and can be expressed as follows:

$$\frac{\partial}{\partial t}(\alpha_{\mathrm{l}}\rho_{\mathrm{l}}k) + \nabla\cdot(\alpha_{\mathrm{l}}\rho_{\mathrm{l}}\vec{u}_{\mathrm{l}}k) = \nabla\cdot\left[\alpha_{\mathrm{sl}}\left(\mu_{\mathrm{l}} + \frac{\mu_{tl}}{\sigma_k}\right)\nabla k\right] + \alpha_{\mathrm{l}}P_{\mathrm{l}} - \alpha_{\mathrm{l}}\rho_{\mathrm{l}}\varepsilon \tag{13}$$

$$\frac{\partial}{\partial t}(\rho_{\mathrm{sl}}\alpha_{\mathrm{l}}\varepsilon) + \nabla\cdot(\alpha_{\mathrm{l}}\rho_{\mathrm{l}}\vec{u}_{\mathrm{l}}\varepsilon) = \nabla\cdot\left[\alpha_{\mathrm{l}}\left(\mu_{\mathrm{l}} + \frac{\mu_{tl}}{\sigma_\varepsilon}\right)\nabla\varepsilon\right] + \alpha_{\mathrm{l}}\frac{\varepsilon}{k}(C_{\varepsilon 1}P_{\mathrm{l}} - C_{\varepsilon 2}\rho_{\mathrm{l}}\varepsilon) \tag{14}$$

where $C_{\varepsilon 1}$, $C_{\varepsilon 2}$, $\sigma_k$, $C_\mu$ and $\sigma_\varepsilon$ are parameters in the standard $k$–$\varepsilon$ model and the following values are selected: $C_{\varepsilon 1}$ = 1.45, $C_{\varepsilon 2}$ = 1.9, $C_\mu$ = 0.09, $\sigma_k$ = 1.0, and $\sigma_\varepsilon$ = 1.3. The turbulent viscosity of liquid phase, $\mu_{tl}$, is modeled using the Sato enhanced turbulence model (Sato and Sadatomi, 1981) as below:

$$\mu_{tl} = \mu_{tl,s} + \mu_{tl,b} \tag{15}$$

where $\mu_{\mathrm{tl,s}}$ is the conventional shear-induced turbulent viscosity, which is obtained by the standard k–ε model as:

$$\mu_{tl,s} = C_\mu \rho_{\mathrm{l}} \frac{k^2}{\varepsilon} \qquad (C_\mu \text{ is a constant}) \tag{16}$$

and $\mu_{tl,b}$ is a bubble-induced component of turbulent viscosity given by:

$$\mu_{\mathrm{tl,b}} = C_{\mu,\mathrm{b}} \rho_{\mathrm{l}} \alpha_{\mathrm{g}} d_{\mathrm{b}} \left|\vec{u}_{\mathrm{g}} - \vec{u}_{\mathrm{l}}\right| \tag{17}$$

A zero equation model is used for calculating the gas phase turbulence (Bartrand et al, 2009; Panneerselvam et al, 2008), in which the gas turbulent viscosity is proportional to that of the liquid phase:

$$\mu_{\mathrm{tg}} = \frac{\rho_{\mathrm{g}}}{\rho_{\mathrm{l}}} \frac{\mu_{\mathrm{tl}}}{\sigma_{\mathrm{t}}} \tag{18}$$

where $\sigma_{\mathrm{t}}$ is a turbulent Prandtl number relating the gas phase kinematic eddy viscosity ($\mu_{tg}$) to the kinematic eddy viscosity of the liquid phase ($\mu_{tl}$).

### 2.3 MUSIG model

The Multiple Size Group (MUSIG) model based on the gas bubble population model is employed to handle polydispersed bubbles in this simulation. One attribute of polydispersed multiphase flow is that different sizes of the dispersed phase interact with each other through the mechanisms of breakup and coalescence (Bhole et al, 2008; Jia et al, 2007; Zhang et al, 2010a). This MUSIG model considers several bubble classes with different diameters ($d_i$), which can be represented by an equivalent phase with a Sauter mean diameter ($d_{\mathrm{b}}$). Let $n(q, t)$ stands for the number density of gas bubbles of size $q$ at time $t$, population balance equations can be described as:

$$\frac{\partial n(q,t)}{\partial t} + \nabla\cdot(u(q,t)n(q,t)) = B_{\mathrm{B}} - D_{\mathrm{B}} + B_{\mathrm{C}} - D_{\mathrm{C}} \tag{19}$$

where $B_{\mathrm{B}}$, $D_{\mathrm{B}}$, $B_{\mathrm{C}}$, and $D_{\mathrm{C}}$ are the birth rate due to breakup of larger bubbles, the death rate due to breakup into smaller bubbles, the birth rate due to coalescence of smaller bubbles, and the death rate due to coalescence with other bubbles, respectively. These rates may further be expressed as:

$$B_{\mathrm{B}} = \int_q^\infty g(w;q)n(w,t)\mathrm{d}w \tag{20}$$

$$D_{\mathrm{B}} = n(q,t)\int_0^q g(q;w)\mathrm{d}w \tag{21}$$

$$B_{\mathrm{C}} = \frac{1}{2}\int_0^q Q(q-w;w)n(q-w,t)n(q,t)\mathrm{d}w \tag{22}$$

$$D_{\mathrm{C}} = n(q,t)\int_0^\infty Q(q;w)n(w,t)\mathrm{d}t \tag{23}$$

where $g(q;w)$ stands for the specific breakup rate, and $Q(q;w)$ for the specific coalescence rate.

For break-up of bubbles in turbulent dispersion, the theoretical model developed by Luo and Svendsen (1996) is employed. This model is based on the theories of isotropic turbulence and probability, and significantly it contains no unknown or adjustable parameters. For the coalescence of two bubbles, the theoretical model developed by Prince and Blanch (1990) is utilized.

## 3 Numerical details

Fig. 2a shows the mesh topology of the loop section. A hybrid mesh topology technique is employed in this study. More detailed information about the mesh topology technique can be found in elsewhere (Lu et al, 2009). Boundary conditions, initial conditions and iteration scheme are set for the numerical simulations using the ANSYS CFX 10.0

software package (ANSYS, 2005). At the gas and liquid inlets, gas and liquid velocities are set according to the experimental input. At the liquid outlet, liquid velocity is assigned to be same as the experimental data. At the gas outlet, degassing condition is used. Along the walls, gas and liquid are treated as free-slip and no-slip, respectively. Initially, the reactor is filled with stationary liquid. Ten initial bubble classes with the diameters ranging from 0 to 8 mm and size fraction of 0.01, 0.07, 0.17, 0.30, 0.21, 0.11, 0.07, 0.04, 0.019 and 0.001 are employed according to the experimental measurements by Zhang et al (2010b). The gas superficial velocity and liquid circulation velocity used are 0.031 m/s and 0.030 m/s respectively in all the simulations. Air at 25 °C with a density of 1.205 kg/m$^3$ and a viscosity of $1.83\times10^{-5}$ Pa·s is used as the gas phase, and water with a density of 998.2 kg/m$^3$ and viscosity of $1.005\times10^{-3}$ Pa·s as the liquid phase for all simulations.

## 4 Results and discussion

The internal loop reactor is generally divided into four regions, namely the riser or draft tube region, the gas-liquid separation region, the annulus region and the bottom region (Luo and Al-Dahhan, 2008; Talvy et al, 2005). Two extra regions have to be considered after an external liquid circulation is introduced (Liu et al, 2007; Lu et al, 2009; Zhang et al, 2010b). Following the above studies, the combined loop reactor is divided into six regions as shown in Fig. 2b, which are bottom region, gas-distributor action region, downcomer-tube action region, upper draft-tube region, gas-liquid separation region and annular region.

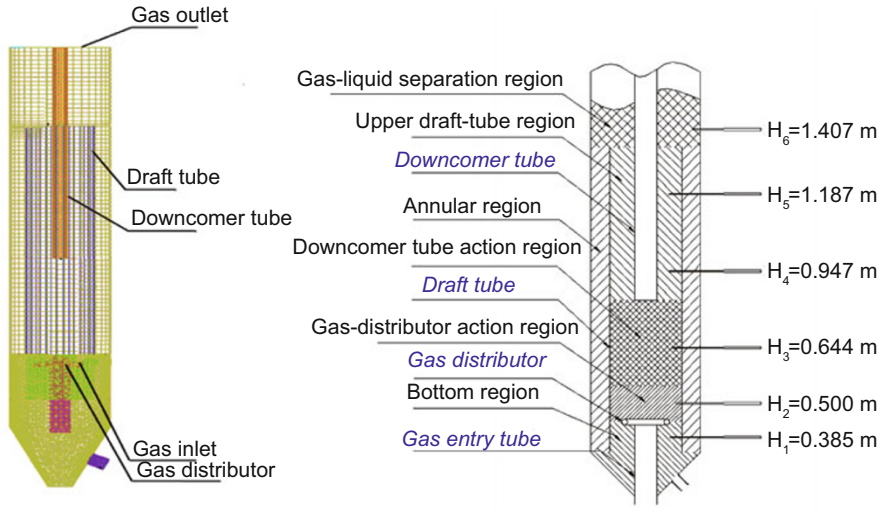


(a) Mesh topology (b) Regions

**Fig. 2** Schematic diagram of the internal loop reactor

### 4.1 Function of the draft tube

As a draft tube is the main feature of the inner loop reactor compared to the traditional bubble column, the effect of the draft tube on the local hydrodynamics of the gas-liquid flow is examined. Figs. 3 and 4 present the liquid and gas velocity vectors in the reactor using a draft tube of diameter 0.192 m. It is found that by fitting a draft tube, liquid and gas are able to pass through a full cycle within the reactor. Liquid moves upward with a relatively high velocity in the centre of the draft tube, which is quite similar to that in a traditional bubble column (Jin et al, 2007). This movement indicates that the the average axial liquid velocity has increased and a better mixing has occurred.

Moreover, the gas holdup and the bubble size distribution are indicators of better performance in the draft tube reactor. As seen in Fig. 5b, the gas holdup in the upper draft-tube region and gas-liquid separation region increases when the draft tube is included in the reactor. This results in higher gas holdup in the annular region because once gas bubbles reach the top of the reactor, a large proportion of gas bubbles disengage while the rest are drawn downward into the annular region as shown in Fig. 4. The bubble size distribution shown in Fig. 6 further validates the benefit of the draft tube. Due to a dramatic increase in the bubble breakage, small size bubbles are formed and size distribution becomes uniform. Therefore, the mass transfer rate is highly enhanced in the reactor due to the larger interfacial surface area of these smaller bubbles.

### 4.2 Effect of draft tube diameter

An important parameter in designing the combined loop reactor with a draft tube is its diameter. In this work, three draft tube diameters of 0.192 m, 0.212 m and 0.236 m were employed to investigate the effect of draft tube geometry on hydrodynamics in the gas-liquid two-phase flow, corresponding to $D_T/D$ = 0.676, 0.746 and 0.831 (where $D_T$ is diameter of the draft tube and $D$ is diameter of column).

As shown in Fig. 7, the liquid velocity vector indicates that there is an overall liquid circulation in the reactor for three draft tube configurations, however, the highest liquid velocity is found in a draft tube reactor with a diameter of 0.192 m, and liquid circulation movement can be clearly seen in the reactor. The bigger the gap between the draft tube and the wall results in the higher the liquid circulation velocity inside the draft tube. By moving towards the reactor wall (the diameter of 0.236 m), the circulation movement becomes weak in the reactor, especially in the gas-liquid separation and bottom regions.

For gas holdup in Fig. 8, it can be found that the difference

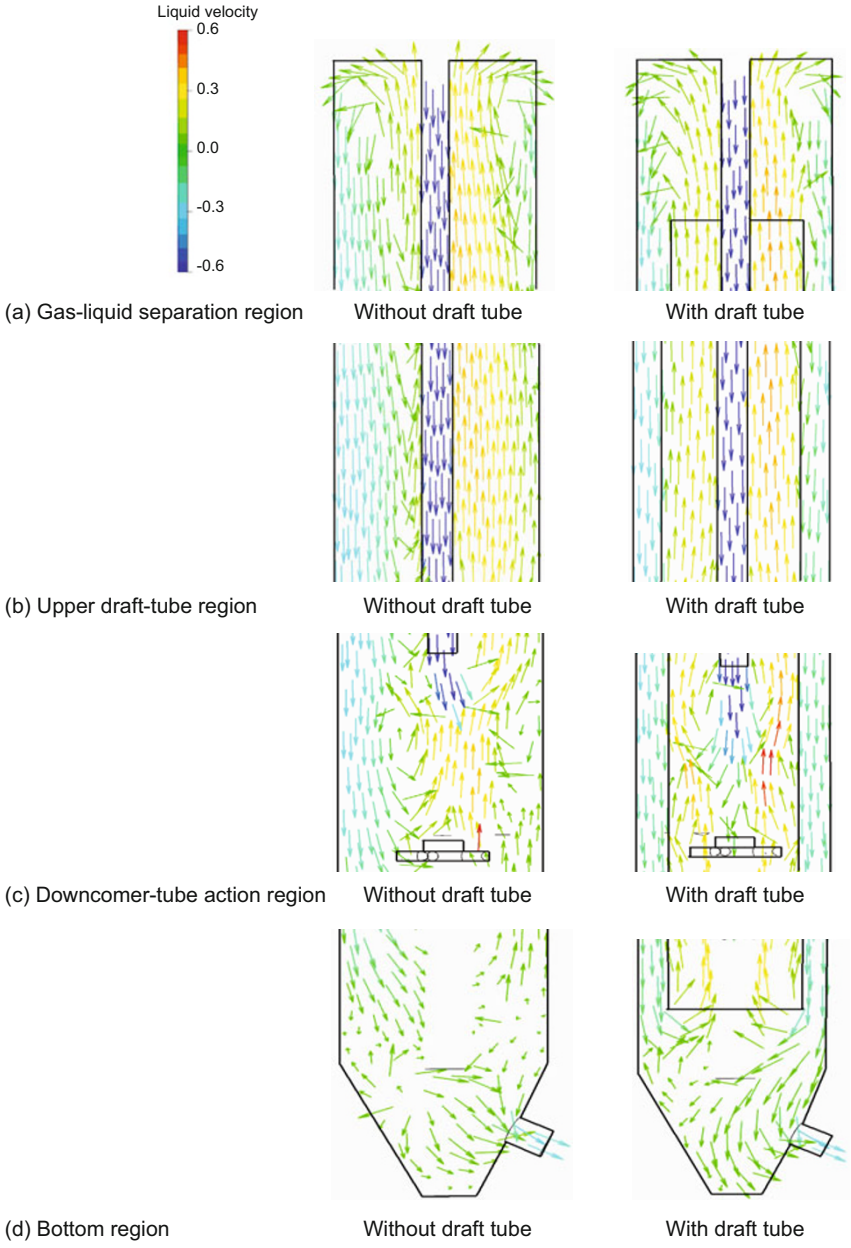


**Fig. 3** Liquid velocity vector in the reactor with and without draft tube

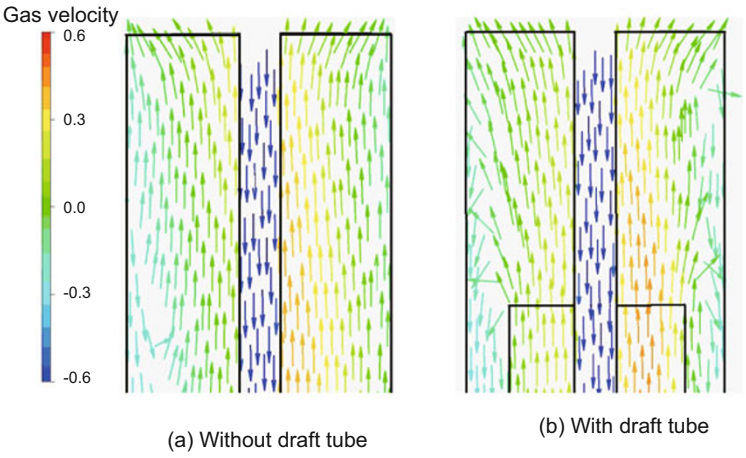


**Fig. 4** Gas velocity vector in reactors with and without draft tube

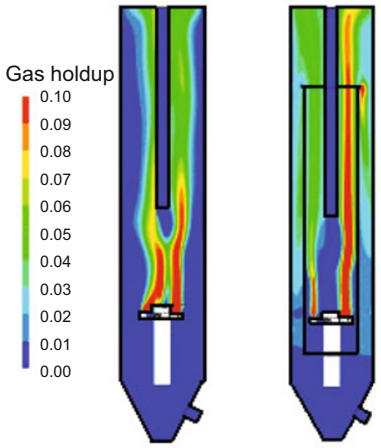


**Fig. 5** Gas holdup distribution in reactors with and without a draft tube

in gas holdup between the draft tube and annular regions is clearly seen as $D_T/D$ increases (Saez et al, 1995), which means a smaller draft tube diameter leads to an increase in the entrainment of gas bubbles to the downcomer compared with larger diameters. Moreover, bubbles are smaller and uniform distributed when the draft tube has a diameter of 0.192 m compared to the bigger ones as shown in Fig. 9. Similarly, Hwang and Fan (1986) found that the draft tube of 7.62 cm inside diameter results in the highest overall gas holdup compared to the other two diameters of 10.16 and 12.7 cm. However, the draft tube can not be too small. Given the same gas flow rate, the gas volume fraction increases sharply in such a small liquid volume with a narrow draft tube, which leads to an increase in gas bubble coalescence rate. Therefore, large gas bubbles form and escape from the surface of the reactor, reducing the gas holdup in the annular region.

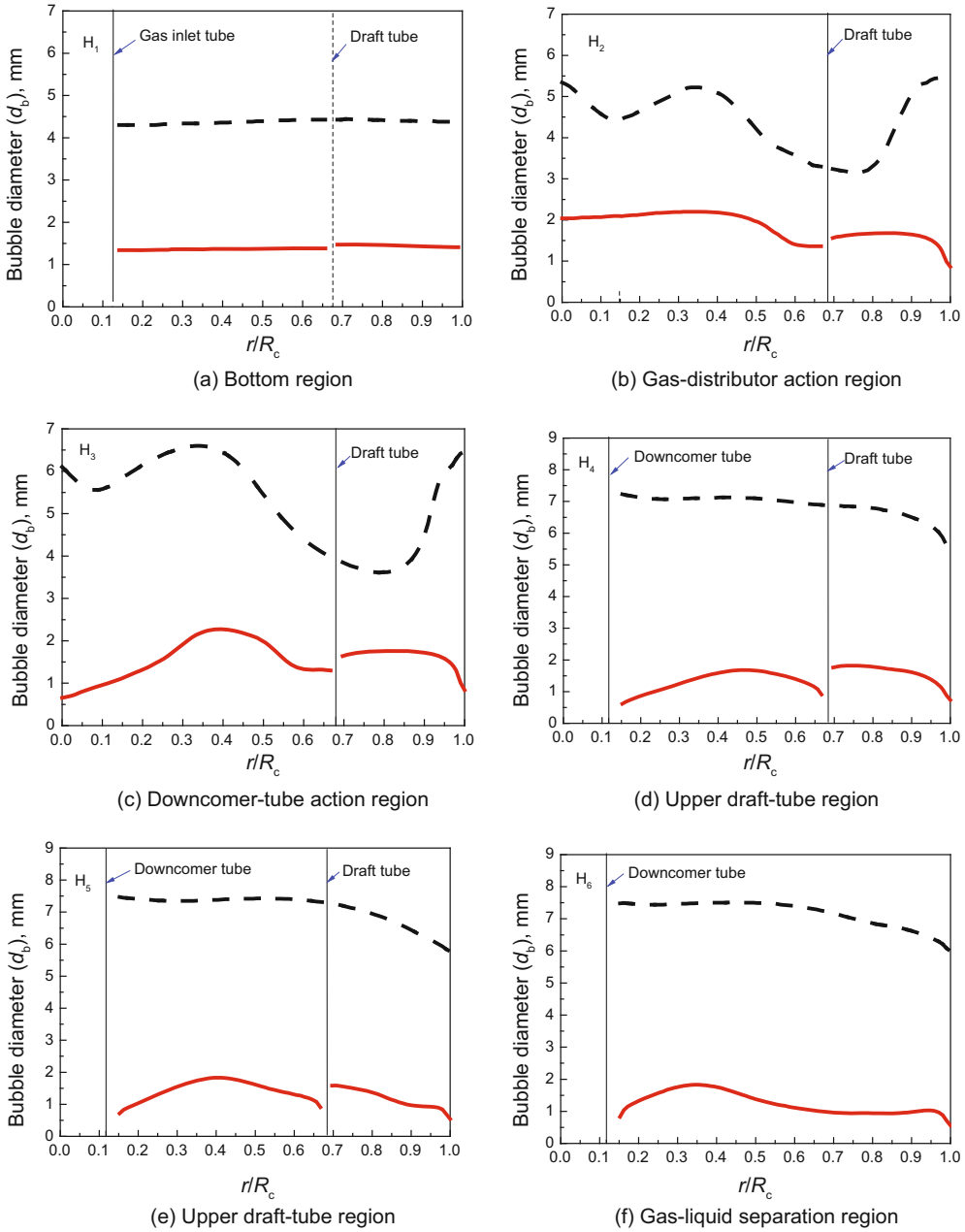


Dash line: without draft tube; Solid line: with draft tube

**Fig. 6** Bubble size distribution with and without a draft tube

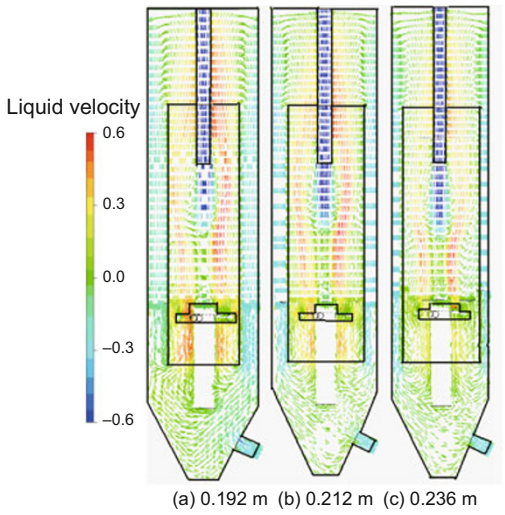


**Fig. 7** Liquid velocity vector in the reactor with different draft tube diameters

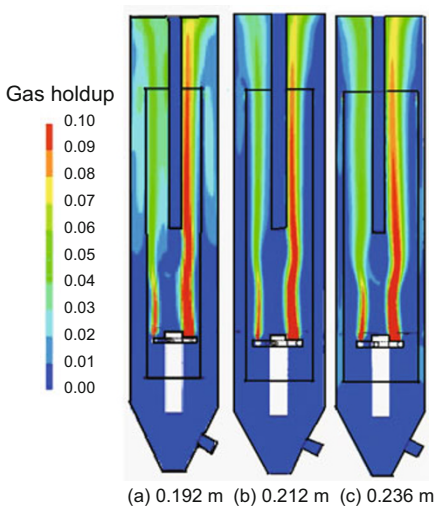


**Fig. 8** Gas holdup with different draft tube diameters

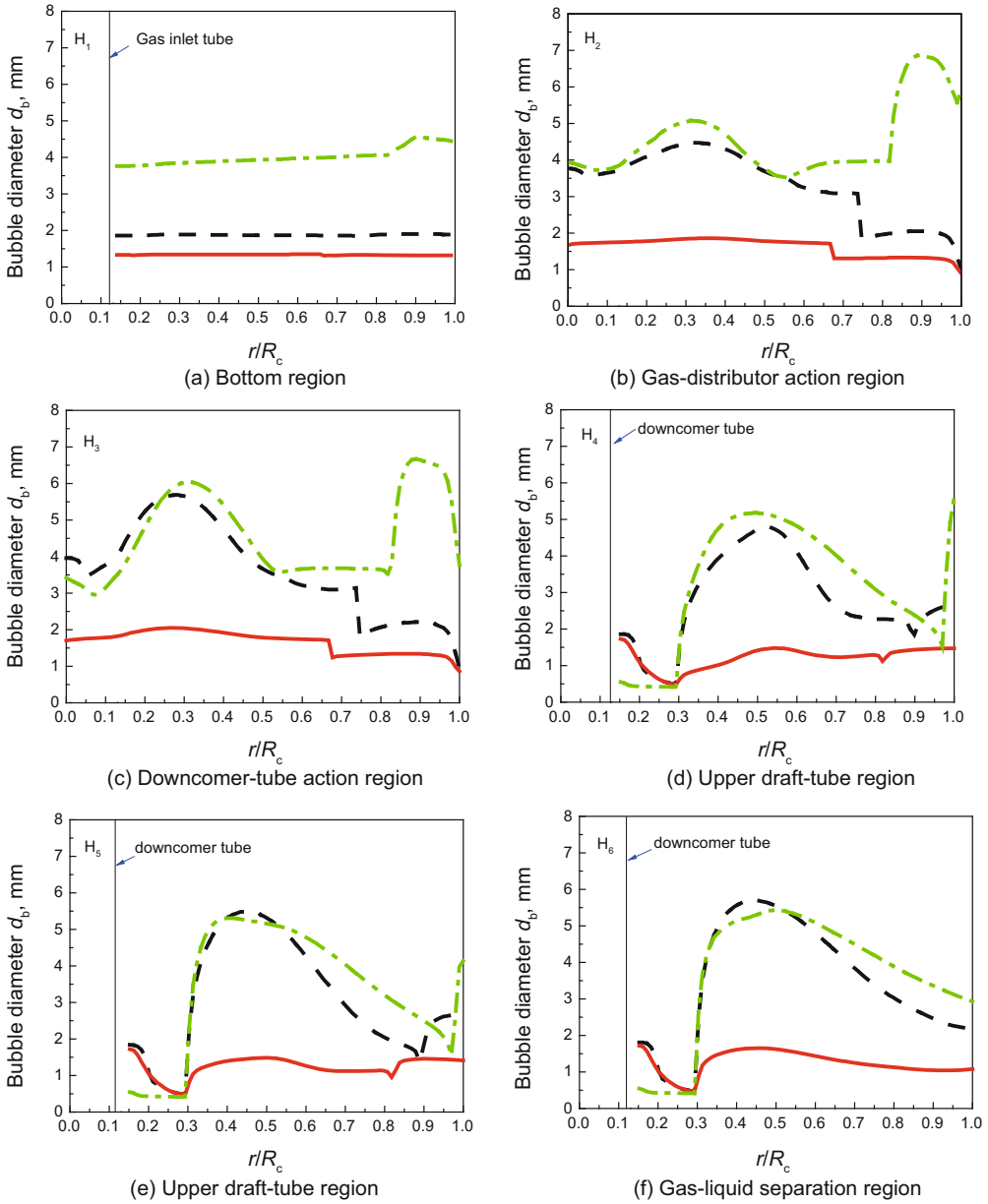


Solid line: 0.192 m; Dash line: 0.212 m; Dash dot line: 0.236 m

**Fig. 9** Bubble size distribution in the reactor with different draft tube diameters

### 4.3 Effect of the draft tube axial location

Two axial locations of the draft tube are compared to investigate the effect of axial location on hydrodynamics in the reactor. One location is 0.17 m beneath the gas distributor, and the other is 0.05 m above the gas distributor.

The liquid velocity vectors at the bottom region of the reactor in Fig.10a demonstrate no liquid circulation when the draft tube is placed above the gas distributor. However, by relocating the draft tube in a lower position, liquid circulation becomes clear (Fig.10b). This is in agreement with a previous report that the stability of the circulation is disrupted if the draft tube is positioned too high above the bottom of the reactor (Saez et al, 1995). From Fig. 11, it can be clearly seen that the gas holdup in the case of the draft tube at a lower position is much higher both inside the draft tube and in the annular region than that for the draft tube at a higher position. This result can be further confirmed by the radial profile of the local gas holdup distribution in the four main regions as shown in Fig.12. Hwang and Fan (1986) also found that

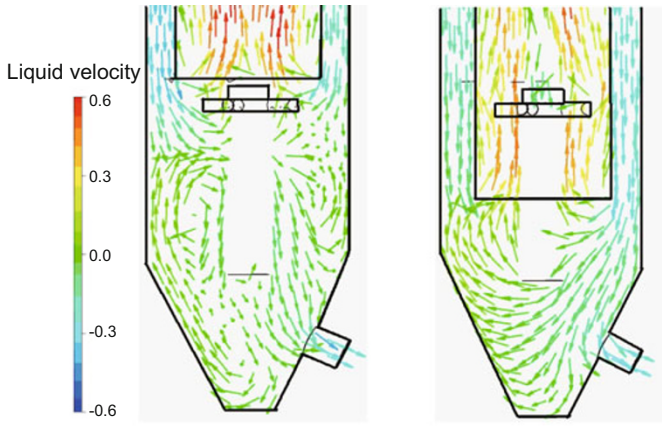


(a) 0.05 m above the gas distributor (b) 0.17 m beneath the gas distributor

**Fig. 10** Liquid velocity vector in the reactors with different axial positions of draft tube

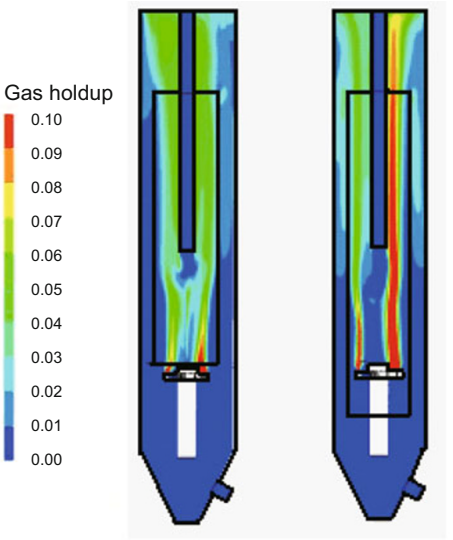


(a) 0.05 m above the gas distributor (b) 0.17 m beneath the gas distributor

**Fig. 11** Gas holdup in the reactors with different axial positions of draft tube

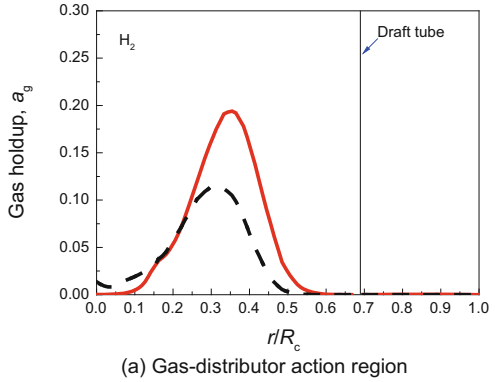


(a) Gas-distributor action region

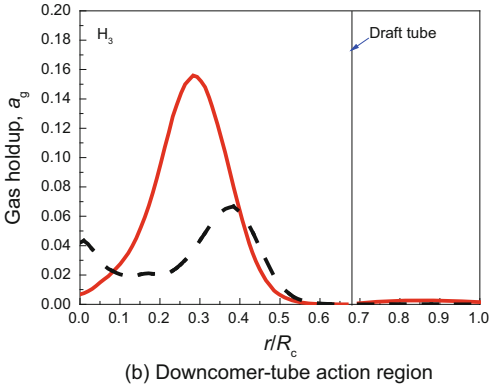


(b) Downcomer-tube action region

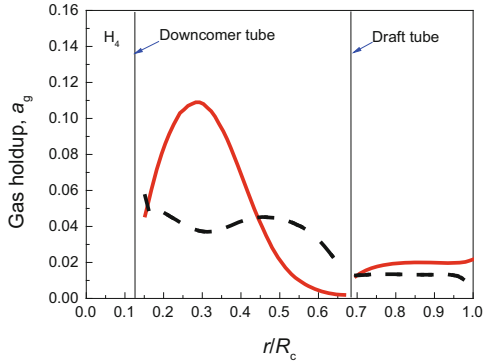


(a) Up per draft-tube region

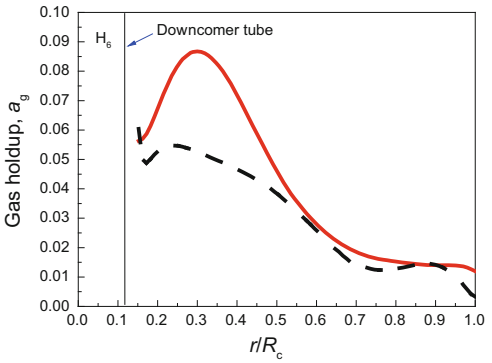


(b) Gas-liquid separation region

Solid line: 0.17 m beneath the gas distributor; Dash line: 0.05 m above the gas distributor

**Fig. 12** Gas holdup distribution in the reactors with different axial positions of draft tube

the highest overall gas holdup is achieved at a relative lower bottom spacing of 1.27 cm compared to other three bottom spacings of 0.44, 2.54 and 5.08 cm.

For the gas bubble size distribution as shown in Fig. 13, smaller bubbles with a diameter less than 2 mm are found when the draft tube is at a lower position (Fig. 13a). In contrast, much larger bubbles are found when the draft tube is at a higher position, especially in the upper draft tube and gas-liquid separation regions due to coalescence (Fig. 13b). Therefore, the conclusion can be drawn that varying the axial position of the draft tube can efficiently control the hydrodynamic behavior of the combined loop reactor.

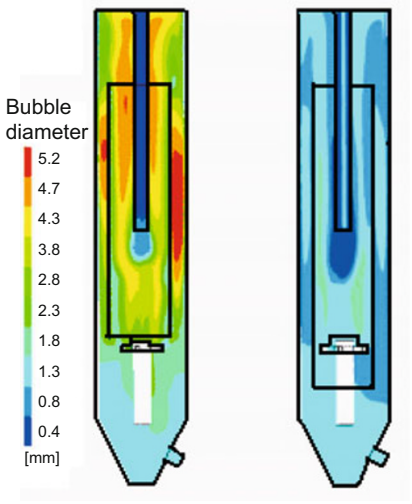


(a) 0.05 m above the gas distributor (b) 0.17 m beneath the gas distributor

**Fig. 13** Bubble size distribution in the reactors with different axial positions of draft tube

## 5 Conclusions

In order to discover the influence of the internals on the hydrodynamics of gas-liquid flow behavior in the internal loop reactor with external liquid circulation, flow pattern, gas holdup and bubble size distribution are simulated by the CFD-PBE coupled model. In view of the results in the current work, the following conclusions are obtained:

1) The function of the draft tube is confirmed by the enhanced liquid circulation, enlarged and more uniform gas holdup, and reduced bubble diameter and narrow size distribution.

2) A draft tube with diameter of 0.192 m has been chosen as the optimized diameter in the gas-liquid flow of our specific reactor because the highest liquid velocity, gas holdup and smallest gas bubbles are obtained, which are helpful to the mass transfer and reaction of the reactor.

3) The axial position of the draft tube can efficiently control the hydrodynamic behavior of this combined loop reactor. Locating the draft tube below the gas distributor gets the best performance from the reactor.

## Acknowledgements

Financial support from the Central Universities (12QN02), National Natural Science Foundation of China (51025624 and 51076043), and 111 Project (B12034) is gratefully acknowledged. We also thank Mr. Qin Yumin for his contribution in the paper.

### Nomenclatures

| | |
|---|---|
| $A_{ij}$ | Net interfacial area between the phases, $m^2$ |
| $B$ | Birth source, $kg/m^3$ s |
| $C_D$ | Drag coefficient |
| $C_{TD}$ | Momentum transfer coefficient for interface drag force |
| $d_b$ | Mean bubble diameter, m |
| $D$ | Diameter of the reactor, m |
| $D_B$ | Death rate due to breakup into smaller bubbles |
| $D_C$ | Death rate due to coalescence with other bubbles |
| $D_T$ | Diameter of the draft tube, m |
| $Eö$ | Eötvös number |
| $F_i$ | Total interfacial force, N |
| $g$ | Acceleration due to gravity, $m/s^2$ |
| $g(m; \varepsilon)$ | Specific breakup rate, 1/s |
| $h$ | Axial height of the reactor, m |
| $k$ | Turbulence kinetic energy per unit mass, $m^2/s^2$ |
| $m$ | Mass, kg |
| $M$ | Morton number, dimensionless |
| $N$ | Number density, $1/m^3$ |
| $P$ | Pressure, Pa |
| $q$ | Bubble size, m |
| $Q(m; \varepsilon)$ | Specific coalescence rate, 1/s |
| $r$ | Radial position of the loop reactor, m |
| $R_c$ | Radius of the loop reactor, m |
| $u$ | Velocity, m/s |
| $u_T$ | The terminal velocity of bubble, m/s |
| $w$ | Bubble size, m |

**Greek letters**

| | |
|---|---|
| $\alpha$ | Volume fraction |
| $\varepsilon$ | Turbulence dissipation rate, $m^2/s^3$ |
| $\mu$ | Viscosity, kg /m·$s^2$ |
| $\mu_{tl,b}$ | Bubble-induced component of turbulent viscosity, kg/(m·s) |
| $\mu_{tl,s}$ | Conventional shear-induced turbulent viscosity, kg/(m·s) |
| $v$ | Kinematic viscosity, $m^2/s$ |
| $\rho$ | Density, $kg/m^3$ |
| $\sigma$ | Surface tension, N/m |

**Subscripts**

| | |
|---|---|
| $b$ | Bubble |
| $g$ | Gas phase |
| $l$ | Liquid phase |
| $t$ | Turbulent |

## References

ANSYS Incorported, ANSYS CFX-Solver Release 10.0, Canada: Ansys Canada Ltd, 2005

Ayed H, Chahed J and RoigV. Hydrodynamics and mass transfer in a turbulent buoyant bubbly shear layer. AIChE Journal. 2007. 53(11): 2742-2753

Bartrand T A, Farouk B and Haas C N. Countercurrent gas/liquid flow and mixing: Implications for water disinfection. International Journal of Multiple Flow. 2009. 35(2): 171-184

Bhole M R and Joshi J B, Ramkrishna D. CFD simulation of bubble columns incorporating population balance modeling. Chemical Engineering Science. 2008. 63(8): 2267-2282

Chen P, Sanyal J and Dudukovic M P. Numerical simulation of bubble columns flows: effect of different breakup and coalescence closures. Chemical Engineering Science. 2005. 60(4): 1085-1101

Clift R, Grace J R and Weber M E. Bubbles, Drops and Particles. New York: Academic Press. 1978

Deng Z H, Wang T F, Zhang N, et al. Gas holdup, bubble behavior and mass transfer in a 5m high internal-loop airlift reactor with non-Newtonian fluid. Chemical Engineering Journal. 2010. 160(2): 729-737

Dhotre M T and Joshi J B. Design of a gas distributor: three-dimensional CFD simulation of a coupled system consisting of a gas chamber and a bubble column. Chemical Engineering Journal. 2007. 125(3): 149-163

Gandhi A B, Gupta P P, Joshi J B, et al. Development of unified correlations for volumetric mass-transfer coefficient and effective interfacial area in bubble column reactors for various gas-liquid systems using support vector regression. Industrial & Engineering Chemistry Research. 2009. 48(9): 4216-4236

Giovannettone J P and Gulliver J S. Gas transfer and liquid dispersion inside a deep airlift reactor. AIChE Journal. 2008. 54(4): 850-861

Hekmat A, Amooghin A E and Moraveji M K. CFD simulation of gas-liquid flow behaviour in an air-lift reactor: determination of the optimum distance of the draft tube. Simulation Modelling Practice and Theory. 2010. 18(7): 27-945

Heyouni A, Roustan M and Do-Quang Z. Hydrodynamics and mass transfer in gas-liquid flow through static mixers. Chemical Engineering Science. 2002. 57: 325-333

Hwang S J and Fan L Sh. Some design considerations of a draft tube gas-liquid-solid spouted bed. Chemical Engineering Journal. 1986. 33(1): 49-56

Jia X Q, Wen J P, Zhou H L, et al. Local hydrodynamics modeling of a gas-liquid-solid three-phase bubble column. AIChE Journal. 2007. 53(9): 2221-2231

Jin H B, Yang S H, Wang M, et al. Measurement of gas holdup profiles in a gas liquid cocurrent bubble column using electrical resistance tomography. Flow Measurement and Instrumentation. 2007. 18(5-6): 191-196

Koide K, Kurematsu K, Iwamoto S, et al. Gas holdup and volumetric liquid-phase mass transfer coefficient in bubble column with draught tube and with gas distribution into tube. Journal of Chemical Engineering of Japan. 1983. 16(5): 413-419

Krishna R, Urseanu M I, van Baten J M, et al. Influence of scale on the hydrodynamics of bubble columns operating in the churn-turbulent regime: experiments vs. Eulerian simulations. Chemical Engineering Science. 1999. 54(21): 4903-4911

Liu M X, Lu C X, Shi M X, et al. Hydrodynamics and mass transfer in a modified three-phase airlift loop reactor. Petroleum Science. 2007. 4(3): 91-96

Lopez de Bertodano M. Turbulent bubbly flow in a triangular duct. Ph. D. Thesis. New York: Rensselaer Polytechnic Institute. 1991

Lu C X, Qi N N, Zhang K, et al. Experiment and CFD simulation on gas holdup characteristics in an internal loop reactor with external liquid circulation. International Journal of Chemical Reactor Engineering. 2009. 7: A3

Luo H P and Al-Dahhan M H. Local characteristics of hydrodynamics in draft tube airlift bioreactor. Chemical Engineering Science. 2008. 63(11): 3057-3068

Luo S M and Svendsen H. Theoretical model for drop and bubble breakup in turbulent dispersions. AIChE Journal. 1996. 42(5): 1225-1233

Nishikawa M, Yonezawa Y, Kayama T, et al. Studies on gas hold-up in gas-liquid spouted vessel. Journal of Chemical Engineering of Japan. 1976. 9(3): 214-219

Panneerselvam R, Savithri S and Surender G D. CFD modeling of gas-liquid-solid mechanically agitated contactor. Chemical Engineering Research and Design. 2008. 86(12): 1331-1344

Prince M and Blanch H. Bubble coalescence and break-up in air-sparged bubble columns. AIChE Journal. 1990. 36(10): 1485-1499

Saez A E, Pironti F F, Medina V R, et al. Effect of draft tube position on the hydrodynamics of a draft tube slurry bubble column. Chemical Engineering Journal. 1995. 60(1-3): 155-160

Sato Y and Sadatomi M. Momentum and heat transfer in two-phase bubble flow-I. International Journal of Multiple Flow. 1981. 7(2): 167-177

Šimčík M, Mota A, Ruzick M C, et al. CFD simulation and experimental measurement of gas holdup and liquid interstitial velocity in internal loop airlift reactor. Chemical Engineering Science. 2011. 66(14): 3268-3279

Talvy S, Cockx A, and Line A. Global modelling of a gas-liquid-solid airlift reactor. Chemical Engineering Science. 2005. 60(22): 5991-6003

Wachi S, Jones A G and Elson T P. Flow dynamics in a draft tube bubble column using various liquids. Chemical Engineering Science. 1991. 46(2): 657-663

Zhang K, Song H S, Sun D K, et al. Low-temperature methanol synthesis in a circulating slurry bubble reactor. Fuel. 2003. 82(2): 233-237

Zhang K and Zhao Y L. A scale-up strategy for low-temperature methanol synthesis in a circulating slurry bubble reactor. Chemical Engineering Science. 2006. 61(5): 1459-1469

Zhang H, Zhang K and Fan S D. CFD simulation coupled with population balance equations for aerated stirred bioreactors. Engineering in Life Science. 2010a. 9(6): 421-430

Zhang K, Qi N N, Jin J Q, et al. Gas holdup and bubble dynamics in a three-phase internal loop reactor with external slurry circulation. Fuel. 2010b. 89(7): 1361-1369

**(Edited by Zhu Xiuqin)**